# **Solvent-Solvent Correlations across Graphene: The Effect of Image Charges**

Neda Ojaghlou<sup>a</sup>, Dusan Bratko<sup>a</sup>, Mathieu Salanne<sup>b</sup>, Mahdi Shafiei<sup>a</sup>, and Alenka Luzar<sup>a</sup>

**ABSTRACT**: Wetting experiments show *pure* graphene to be weakly hydrophilic, but its contact angle (CA) also reflects the character of the supporting material. Measurements and Molecular Dynamics simulations on suspended and supported graphene often reveal a CA reduction due to the presence of the supporting substrate. A similar reduction is consistently observed when graphene is *wetted* from both sides. The effect has been attributed to transparency to molecular interactions across the graphene sheet, however, the possibility of substrate-induced graphene polarization has also been considered. Computer simulations of CA on graphene have so far been determined by ignoring the material's conducting properties. We improve the graphene model by incorporating its conductivity according to the Constant Applied Potential Molecular Dynamics. Using this method, we compare the wettabilities of suspended graphene and graphene supported by water by measuring the CA of cylindrical water drops on the sheets. The inclusion of graphene conductivity and concomitant polarization effects lead to a lower CA on suspended graphene but the CA reduction is significantly bigger when the sheets are also wetted from the opposite side. The stronger adhesion is accompanied by a profound change in the correlations among water molecules across the sheet. While partial charges on water molecules interacting across an insulator sheet attract charges of the opposite sign, apparent attraction among like charges is manifested across the conducting graphene. The change is associated with graphene polarization, as the image charges inside the conductor attract equally signed partial charges of water molecules on both sides of the sheet. Additionally, by using a non-polar liquid (diiodomethane), we affirm a detectable wetting translucency when liquidliquid forces are dominated by dispersive interactions. Our findings are important for predictive modeling toward a variety of applications including sensors, fuel cell membranes, water filtration, and graphene-based electrode materials in high-performance supercapacitors.

**KEYWORDS**: graphene conductivity, image charges, contact angle, wetting transparency, constant applied potential molecular dynamics

<sup>&</sup>lt;sup>a</sup> Department of Chemistry, Virginia Commonwealth University, Richmond, Virginia 23284, United States

<sup>&</sup>lt;sup>b</sup> Sorbonne Université, CNRS, Physico-Chimie des Électrolytes et Nanosystèmes Interfaciaux, Phenix, F-75005 Paris, France

<sup>\*</sup>dbratko@vcu.edu

An atomically thin layer of graphene, a single-atom-thick sheet of sp²-hybridized carbon atoms arranged in a hexagonal honeycomb lattice, exhibits unique mechanical, optical, and electronical properties. <sup>1-8</sup> As a result, graphene has become a subject of intense basic and applied research. <sup>9-15</sup> For example, because of its extraordinary surface to volume ratio, <sup>16,17</sup> experimentalists have suggested graphene-based electrodes can enhance the performance of supercapacitors <sup>17,18</sup> and batteries. <sup>19,20</sup> Extremely thin and electrically conductive, graphene is widely used in biosensors, <sup>21</sup> lab-on-a-chip, fabrication of membranes for water filtration <sup>22</sup> and desalination, manufacture of fuel cells, and microfluidics platforms where graphene is in contact with water, vapor, and analytes. <sup>23,24</sup> Many of the above applications critically depend on the graphene wettability in water. Wetting properties of graphene have been a subject of several theoretical and experimental investigations over the last decade, <sup>25-28</sup> however, fundamental characterization and molecular level understanding of wetting phenomena on graphene remain incomplete. Moreover, an accurate measurement of the contact angle (CA) on graphene is often difficult to accomplish because of defects, airborne contaminants, and oxide formation on the surface.

Contact angle measurements have also revealed a significant dependence of graphene wettability on the supporting substrate, a phenomenon often interpreted as a consequence of graphene transparency to water-substrate interactions.<sup>26, 29-32</sup> For instance, the water static contact angle on neat graphene supported by copper is 44°, while it is 60° for the pyrolytic graphite.<sup>25</sup> The experimental estimate for suspended graphene, on the other hand, has been reported<sup>32</sup> at 85±5°, close to theoretical predictions<sup>28,33,34</sup> of 87°, 90°, and 79°, respectively. The effect is not limited to solid substrates. Comparisons between contact angles on suspended graphene with those measured on graphene fragments supported by water have generally shown increased wettability when graphene was surrounded by water from both sides. Early MD simulations indicated the contact angle of a water droplet on a graphene sheet is about 7° lower when the system is submerged in water.<sup>35</sup> Experiments performed by Checco and his group<sup>32</sup> using graphene on a pillared substrate revealed an even bigger effect. Replacing air between the pillars by water resulted in estimated CA reduction between 19 and 24°. A qualitatively similar effect has been observed with ice or hydrogel support replacing the underlying water.<sup>36</sup> The clear distinction between graphene wettabilities in the presence and absence of supporting substance has important repercussions for the predictions of graphene

properties in dispersions. Theoretical predictions of the effect have mostly focused on direct interactions between water molecules and solid or liquid support on the opposite side of the sheet. Based on the Young-Dupre equation, the contact angle of a graphene-coated substrate should correspond to the adhesion strength associated with combined attraction exerted on the water by graphene and the supporting substrate,  $^{29-32, 37}$  or underlying liquid.  $^{32, 35}$  Using a simple mean-field method for pair-wise additive dipolar and dispersive interactions, Driskill *et al.*  $^{35}$  estimated the contact angle difference  $\Delta\theta$  between graphene platelets supported by water and air to be near -10°.

While the presumed interaction additivity provided a plausible rationale for early experimental observations, it also resulted in considerable quantitative differences between predicted and measured CA in numerous cases. Following comparisons with experiments, ab initio modeling, and classical accounts of multi-body interactions, a number of groups have also discussed substrate-induced changes of the electronic structure of graphene, which in turn affect graphene-water forces and propensity for wetting. 17, 25, 38-41 Distinct but interrelated effects predicted in first principles studies<sup>25, 40-44</sup> include local (atomic) and large-scale polarization events, the shift in graphene Fermi level, and charge transfer between substrates and graphene, all of which can potentially tune graphene's apparent polarity. 45,46 When graphene is supported by a polar liquid like water, polarization effects are expected to play a notable role, however, prohibitive system sizes and slow statistical convergence have so far precluded direct estimates of these effects on wetting properties in ab initio simulations. Atomic polarizabilities of graphene and graphite have been considered in MD calculations with polarizable force fields based on charge-on-spring (Drude oscillator),<sup>38</sup> or OPLS-AAP models.<sup>17, 38,47</sup> Misra and Blankschtein highlighted the importance of the induction energy and associated entropy on the wetting propensity of graphite<sup>39</sup> using a rigorous self-consistent treatment of induced dipolar interactions. Notably they demonstrated that the effect cannot be captured by conventional pairwise-additive approaches with adjusted water/carbon interaction.

First principles calculations show that 'planar graphene acts as a metal along the carbon plane and as semiconductor perpendicular to it,<sup>44</sup> with the *ratio* of the lateral and normal permittivities diverging<sup>44</sup> for sizeable sheets. With the exception of sheet edges (relevant only for small-size sheets), the lateral mobility of  $\pi$  electrons is demonstrated to produce essentially perfect shielding of external electric field<sup>44</sup> in the tangential directions. A similar dielectric

anisotropy<sup>44, 48,49</sup> has been observed in density functional calculations for semi-metal carbon nanotubes (CNT-s).<sup>50</sup> With the transverse components of the permittivity *and* polarizability virtually independent on the band gap,  $\Delta_g$ , and the longitudinal polarizability scaling roughly as  $\Delta_g^{-2}$ , the graphene-like armchair CNT-s, characterized by chiral vectors (m,n) with n=m and vanishing band gap  $\Delta_g$ , featured low transverse but divergent longitudinal polarizabilities.<sup>50</sup> Even in semi-metal zig-zag CNT-s, characterized by chiral vectors (3n,0) and low but *finite* band gaps from  $\sim 0.17$  eV at n=3 to  $\sim 0.04$  eV at n=5, the observed ratio of longitudinal and transverse polarizabilities varied from  $O(10^2)$  to  $O(10^3)$ , respectively.<sup>50</sup> The pronounced polarizability anisotropies in graphene-like (semi-metallic) CNT-s<sup>50</sup> reinforce the observations from single-layer graphene permittivity calculations<sup>44</sup> outlined above. Treating graphene as a conductor<sup>2</sup> is hence expected to capture the dominant features of its polarization and associated induction effects in a polar environment.

So far, contact angle simulations of water on graphene have been performed without explicitly accounting for the material's conductivity. In this paper, we augmented the graphene force field by adding the conductor properties using the fluctuating-charge technique of Constant Applied Potential Molecular Dynamics (CAPMD).51,52 Consistent with first principles calculations,44 the fluctuating carbon atom charges of the CAPMD model eliminate the in-plane components of the electric field associated with the structural fluctuations<sup>53,54</sup> in adjacent water. The induced Gaussian charges on carbon atoms also affect the perpendicular component of local field, shielding the *direct* interactions among partial charges of water molecules at the opposite sides of the carbon layer. In addition to increased propensity to wetting, graphene polarization underlies a qualitative change of correlations among water molecules separated by the sheet. We evaluated the wettability by measuring the contact angle of cylindrical water drops on a conducting graphene sheet. We found that the contact angle of a water droplet on a graphene sheet submerged in water is lower than in the absence of water under graphene. In other words, water-graphene adhesion is stronger when graphene is wetted from both sides. The effect is enhanced when we incorporate graphene conductivity. The greater reduction in the contact angle on a submerged sheet is associated with the indirect, graphene-mediated attraction between the water partial charges of equal sign bridged by the induced (image) charges on the electrically polarized graphene. The mechanism is important for the basic understanding of hydration of thin conducting materials.

Parallel calculations for a nonpolar liquid (diiodomethane) confirm that dispersion forces alone result in a moderate "wetting transparency",<sup>45</sup> however, only two-side wetting by polar solvents proves sensitive to the inclusion of material's conductivity. The effect is of potential importance for *in silico* predictions of graphene wettability by water to optimize applications from sensors to porous electrodes, fuel cell membranes, and water filtration. The conductor properties can also play a role in hydrophobic interactions among dispersed graphitic nanoparticles,<sup>55</sup> which are often used as showcase systems in modeling<sup>56-59</sup> nanoparticle interactions in water.

### RESULTS AND DISCUSSION

To assess the importance of graphene conductivity and associated polarization effects on its wetting propensity, we monitor simulated water nanodrops on a suspended (unsupported) graphene sheet and on a sheet supported by liquid water from the opposite side. In each of the two scenarios, we compare the results for water contact angles, and characteristic structures of hydration water, using a conventional graphene model devoid of atom charges or polarizability with those obtained by accounting for the conductor properties of graphene. The cylindrical droplet shape is used to avoid line tension effects with nanodrop sizes amenable to MD simulations. The model setups are illustrated in Figure 1, and the details are given in the Methods section. The force field treating graphene as an insulator has been described in earlier work.<sup>35</sup> In the present work, the conductivity is incorporated using the method of fluctuating charges from the Constant Applied Potential Molecular Dynamics (CAPMD) developed by Sprik and Siepmann<sup>51</sup> and Madden and coworkers.<sup>52</sup> In this approach, every carbon atom of graphene carries a Gaussian charge distribution  $\rho_j(r-r_j)$  with an integrated charge of  $q_j$  and the fixed Gaussian charge width<sup>52</sup>  $\eta$ .

$$\rho_j(r) = q_j Aex \, p\left(-\left|r - r_j\right|^2 \eta^{-2}\right) \tag{1}$$

where  $r_j$  denotes the atom's position,  $q_j$  is the instantaneous value of the fluctuating charge on atom j, and  $A = \eta^3 \pi^{3/2}$  is the normalization constant. Oxygen and hydrogen atoms of water

molecules carry fixed point charges, with the local charge density  $\rho(r)$  at the position r due to an atom i located at  $r_i$  given by

$$\rho_i(r) = q_i \delta(r - r_i) \tag{2}$$

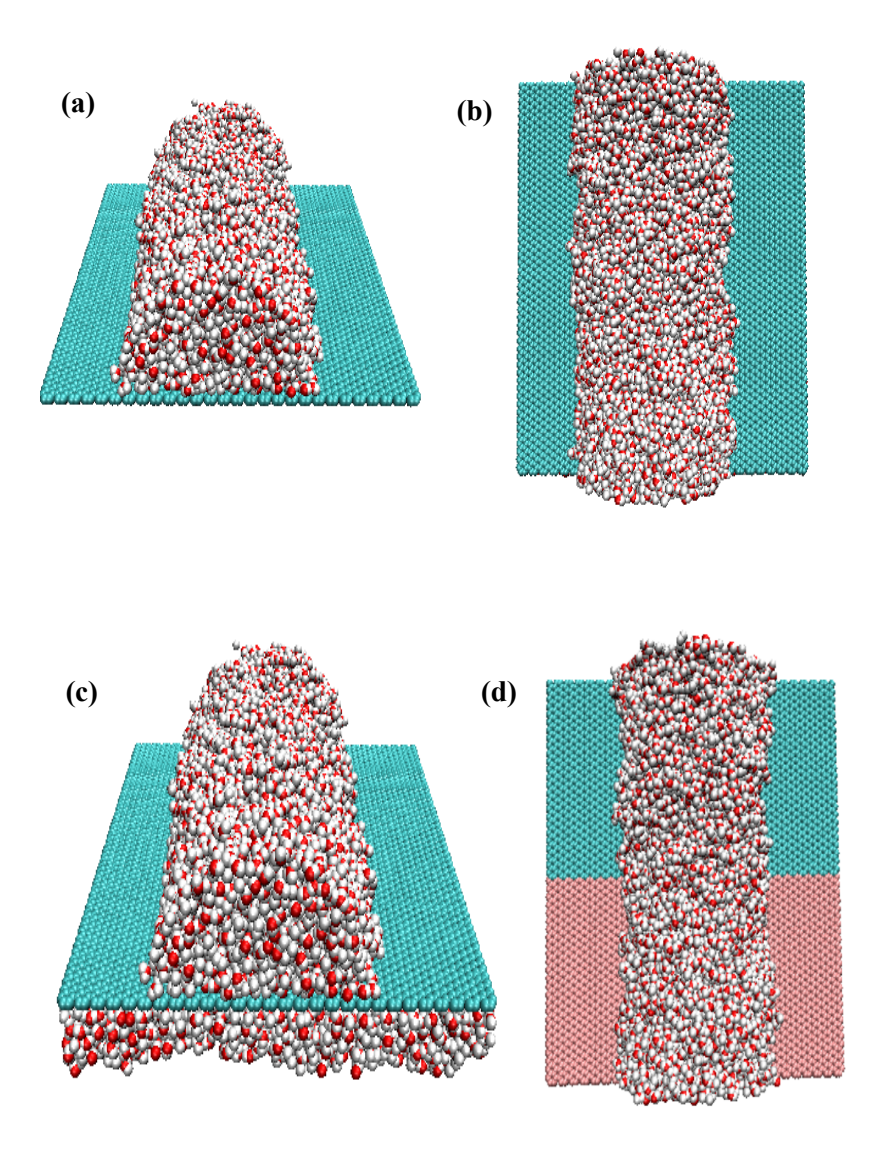


Figure 1: Snapshots of spreading of the semi-infinite hemi-cylindrical water droplet atop insulator without (a-b) or with a layer of water (c) placed below the sheet. The system containing a 6.4·10³ molecule drop on a 5.6·10³ atom graphene sheet is periodically replicated in lateral directions. (d) A snapshot of a cylindrical water droplet atop graphene sheet in CAPMD (See Methods section). The different colors of the graphene surface denote the nominal 'electrodes' of the CAPMD setup at vanishing voltage V.

where  $\rho(r)$  and  $\delta(r - r_j)$  are total charge density and delta function. The total charge density at r is given as the sum of contributions from all carbon atoms (Eq. 1) and partial charges from the water molecules (Eq. 2). The internal columbic energy of the system  $U_c$  is

$$U_{c} = \frac{1}{2} \iint \frac{\rho(r')\rho(r'')dr'dr''}{|r'-r''|}$$
 (3)

To secure a desired electrostatic potential  $V_j^o$  on graphene atoms (typically the imposed electrode potential), carbon charges  $q_j$  undergo a perpetual redistribution responding to the changing configuration of water molecules.<sup>51,52,60</sup> In a general case, the instantaneous charges  $q_j$  are obtained variationally by minimizing the total electrostatic energy  $U_t = U_c - \Sigma_j q_j V_j^o$ . In the present scenario,  $V_j^o$  are set equal to zero for all carbon atoms j and the minimization is carried out subject to the net neutrality condition,  $\Sigma_j q_j = 0$ .

Through perpetual in-plane charge redistributions, the model also provides electrostatic shielding of the perpendicular component of the nonuniform field from the partial charges of water molecules. At the present level of approximation, it does not explicitly account for the finite out-of-plane polarizability<sup>39, 43, 50, 61</sup> of carbon atoms in graphene. Given the two in-plane polarizability components considerably exceed the out-of-plane one already in graphite,<sup>44, 62</sup> and more so in highly anisotropic single-layer graphene<sup>44</sup> and semimetallic CNT-s,<sup>50</sup> this approach is likely to capture the main contribution to the induction energy associated with graphene wetting. A definitive statement would require augmenting the model by drude oscillators but this appears technically challenging *in combination* with the CAPMD approach accounting for the metal-like in plane polarization.

As detailed in the Methods section, we model water molecules using the SPC/E water potential<sup>63</sup> and graphene atoms as Lennard-Jones (LJ) particles. In view of experimental uncertainties in determining the suspended graphene/water interaction,<sup>32, 34, 64,65</sup> we consider three different strengths of carbon interaction with water oxygen atoms,  $\varepsilon_{co}$  (Table 1) with the intermediate strength,  $\varepsilon_{co}\sim0.39$  kJ mol<sup>-1</sup> corresponding to recent experimental<sup>32</sup> and quantum-mechanical simulation<sup>28</sup> estimate for the CA on neat suspended graphene at  $\sim 86\pm3^{\circ}$ . Results for weaker ( $\varepsilon_{co}\sim0.195$  kJ mol<sup>-1</sup>) and stronger ( $\varepsilon_{co}\sim0.52$  kJ mol<sup>-1</sup>) water surface interactions are included to cover the broad range of CA values indicated in independent experiments. Identical

LJ interactions are used in conducting and insulator representations. In describing our results, we refer to the conducting (CAPMD fluctuating-charge) and non-conducting model systems using the terms 'graphene' and 'insulator', respectively.

Table 1: Contact angle  $\theta$  of a cylindrical droplet on the suspended and supported graphene for different values of  $\varepsilon_{co}$ .  $\theta_c$  refers to measurements without a water layer underneath the surface and  $\theta_w$  correspond to a layer of water placed underneath graphene.

$\varepsilon_{co}$	suspended	water-supported	suspended	water-supported
$/kJ \; mol^{-1}$	insulator $\theta_c$	insulator $\theta_w$	graphene $\theta_w$	graphene $\theta_w$
0.1951	127°±1°	120°±1°	118°±1°	105°±1°
0.3913	89°±1°	81°±1°	87°±1°	75°±1°
0.5208	59°±1°	52°±1°	54°±1°	45°±1°

**Graphene/water density profiles.** We begin by describing the structure of hydration layers on both sides of the surface. The oxygen density profiles shown in Figure 2 reveal only a small

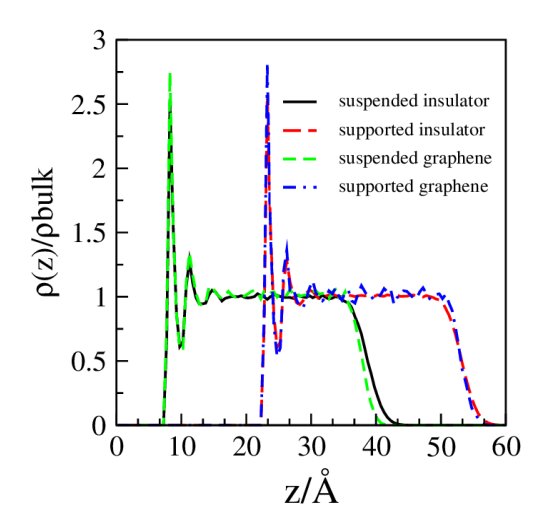


Figure 2: Density profiles of water in the central region of a cylindrical droplet base on the suspended or supported insulator and graphene sheets (modeled by CAPMD) with  $\varepsilon_{co} = 0.3913 \, kJ \, mol^{-1}$ . Black curve: simulation result for the droplet density as function of the height z on the suspended insulator. Red: droplet on the insulator supported by an aqueous layer. Green: droplet on the suspended graphene. Blue: droplet on supported graphene. The densities are normalized by the density inside the bulk portion of the droplet.

difference in the distributions of water molecules on the insulator compared to the graphene sheet. The only detectable difference is seen in the slight increase in the heights of the first hydration peaks for both the suspended and supported graphene relative to those observed with the insulator sheet. A somewhat worse statistics is observed in conductor systems with added degrees of freedom (fluctuating carbon atom charges), especially in the case of graphene supported by water where charge fluctuations are more pronounced (*vide infra*). In Figure 3, we compare the density profiles of water next to strongly hydrophobic and hydrophilic insulator surfaces (Systems 1 and 3 in the 1<sup>st</sup> column in Table 1) on both sides of the submerged graphene

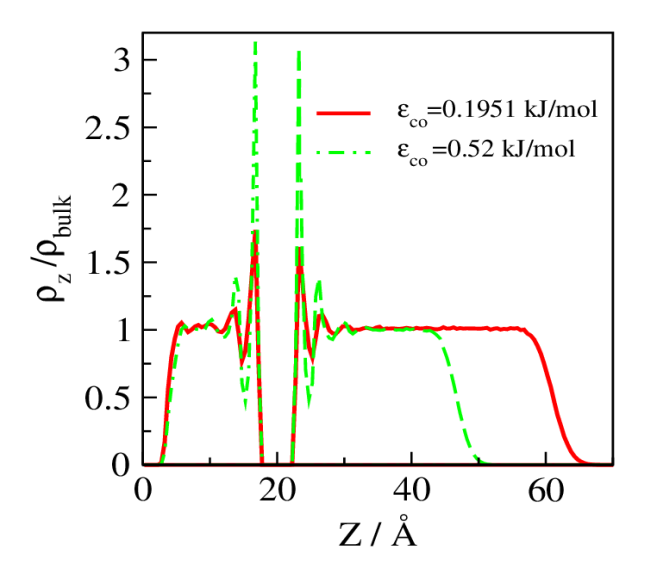


Figure 3: Density profile of water on both side of the insulator surface for  $\varepsilon_{co} = 0.1951 \ or \ 0.5208 \ kJ \ mol^{-1}$ . The plot shows each profile in relation to the z-dimension of the system box. The insulator sheet is placed at  $z = 20 \mbox{Å}$ .

sheet. These results show the 1<sup>st</sup> peak positions at the hydrophobic surfaces are significantly lower and slightly (~ 1Å) withdrawn from the sheets compared to the hydrophilic cases. Water density profiles are essentially identical on both sides of the graphene sheet, the small reduction of the height of the 1<sup>st</sup> peak on the drop side being explained by mild density variation along the radial direction of the droplet's base.

Contact angles. Figure 4 illustrates the time dependence of the dynamic contact angles we extract from the *instantaneous* droplet contours (see Methods section). The curves showing instantaneous contact angles feature appreciable noise due to drop's shape fluctuations, which

are mostly averaged out in the cumulative contact angle results, Table 1. Figure 4-left shows the simulated contact angles of a cylindrical droplet on a suspended graphene sheet obtained using the insulator (black) or conducting graphene (green) models. Figure 4-right compares the CA results for (conducting) graphene in two different situations: (a) suspended sheet with empty space underneath, and (b): supported sheet atop a slab of water. As shown in Table 1, the reduction in contact angle on submerged conducting graphene is between 9°-13°, considerably more than the change of 6°-7° predicted<sup>35</sup> with the insulator model. The comparison between the two different surface models shows that the conductivity of the surface has a smaller effect on the contact angle when the droplet is placed on a suspended sheet.

Table 1 also compares the results of time-averaged contact angles of water on graphene and insulator surfaces for a different set of oxygen-carbon energy parameters  $\varepsilon_{co}$ . These results show that the inclusion of material conductivity is most visible on hydrophobic model surfaces where the related polarization effects present a greater share in the total surface/water attraction. Lastly we note a difference between our results for water on graphene and the original calibration for graphite provided by Werder *et al.*<sup>66</sup> In addition to replacing graphite by graphene, this differences reflect several methodology improvements, the most significant being the use of

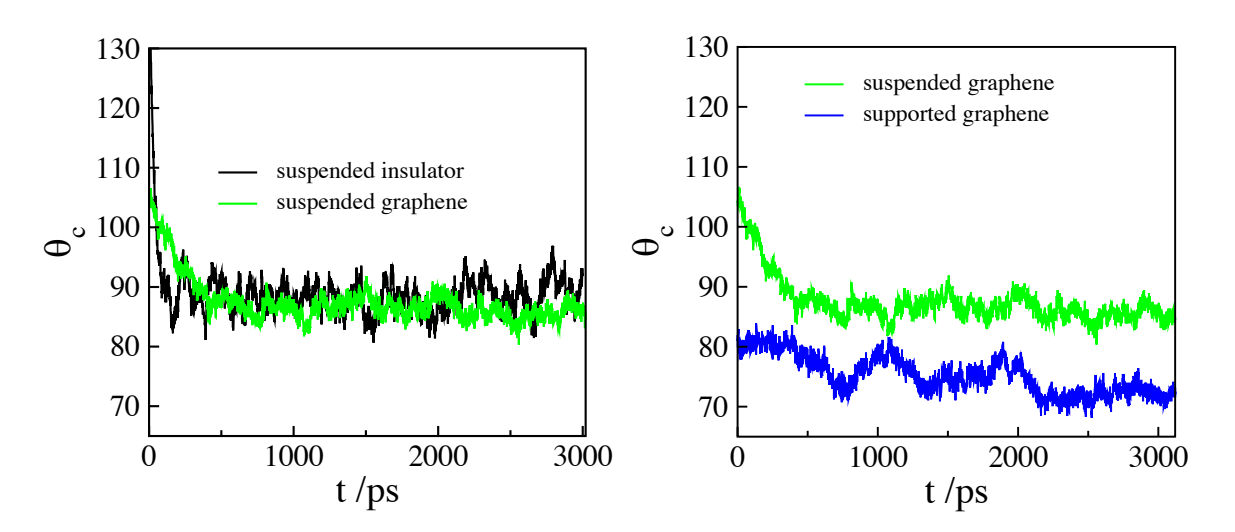


Figure 4: Contact angle vs. time for a cylindrical water droplet on the suspended insulator and graphene sheets (left) and suspended or water-supported graphene sheets (right) for carbonwater interaction strengths  $\varepsilon_{co} = 0.3913 \ kJ \ mol^{-1}$ .

Ewald summation to avoid the cutoff (10 Å in Ref.<sup>66</sup>) of electrostatic interactions, and the choice of cylindrical drop geometry<sup>33</sup> to eliminate the finite-size effects associated with line tension.

Would the results we present change with different water models? Surface tension and associated contact angles of water are known<sup>39, 67,68</sup> to depend on the particular force field but the trends we study appear less sensitive to the particular choice. While calculations of contact angle changes with CAPMD are too costly for comparisons of different water models, we refer to a related study<sup>39</sup> comparing the induction effects on the wetting free energies on graphite for two distinct water potentials, the nonpolarizable SPC/E<sup>63</sup> and polarizable SWM4-NDP model.<sup>69</sup> Interestingly, the induction effects (central to our study) are found virtually insensitive to the applied potential.

Since the model of ref.<sup>39</sup> also includes out-of-plane polarizabilities, it is of interest to include a brief comparison of the magnitudes of induction effects in their study and the present method, which captures only in-plane polarization. When applied to study single-surface wetting, the CAPMD approach yields induction energy and entropy changes  $\Delta U^{\text{ind}} = -7.1 \text{ mJ m}^{-2}$ and  $T\Delta S^{\text{ind}} \sim -2 \text{ mJ m}^{-2}$ , respectively (we estimate the entropic term from the difference between the induction surface energy and the wetting free-energy corresponding to the average contact angle change upon inclusion of polarization effects). The above values are comparable to the induction energy  $\Delta U^{\text{ind}} = -8.4 \text{ mJ m}^{-2}$  and associated entropy reduction  $T\Delta S = -4.4 \text{ mJ m}^{-2}$  observed in ref.<sup>39</sup> when using the polarizability and damping parameters deduced from the polarizability tensor of graphene (Model II in Table 1 of ref.<sup>39</sup>). Incorporation of explicit out-of-plane polarizability could strengthen the attraction and angular restrictions in our model, potentially improving the agreement between energetic and entropic effects from the two approaches. While our code does not support such a calculation in its present form, the moderate energy difference between  $\Delta U^{\text{ind}}$  values from the two models appears compatible with the *relative* magnitudes of in-plane ( $\alpha_{xx}$  and  $\alpha_{yy}$ ) and out-of-plane ( $\alpha_{zz}$ ) polarizabilities<sup>62</sup> adopted in ref.<sup>39</sup>. The induction effects predicted by the two models discussed above can, however, not be directly compared with more prominent energy and entropy changes observed in Model III of ref.<sup>39</sup>, which relies on adjusted polarizability and damping parameters to account for the additional attraction arising from the overlapping charge distributions of solvent and carbon atoms.

**Dipolar correlations across graphene.** To gain a more detailed picture of the orientational polarization of hydration water, in Figure 5 we show the water dipole angle distributions  $p(\cos \varphi)$  for both the suspended and supported insulator and conducting graphene sheets. Here,  $\varphi$  represents the angle between a water dipole and the normal to the graphene surface. We quantify the interfacial polarization in terms of the average dipole of the interfacial molecules  $<\mu(t)>=\frac{1}{N}<\sum_i^N\mu_i(t)>$ , where the sum runs over all water dipoles  $\mu_i$  in the first hydration layer. We define this layer as the region between the surface and the first minimum in the water/surface density profile. As can be seen in Figure 5, in the system with the insulating surface (black and red curves in Figure 5), the presence of the supporting aqueous slab has a strong influence on the orientational polarization in the droplet base. This effect, associated with dipole-dipole interaction across the surface, is essentially screened out when we include graphene conductivity (green and blue curves). As will be shown below, partial molecular charges of the same sign appear attracted to each other across the conducting graphene in contrast to the

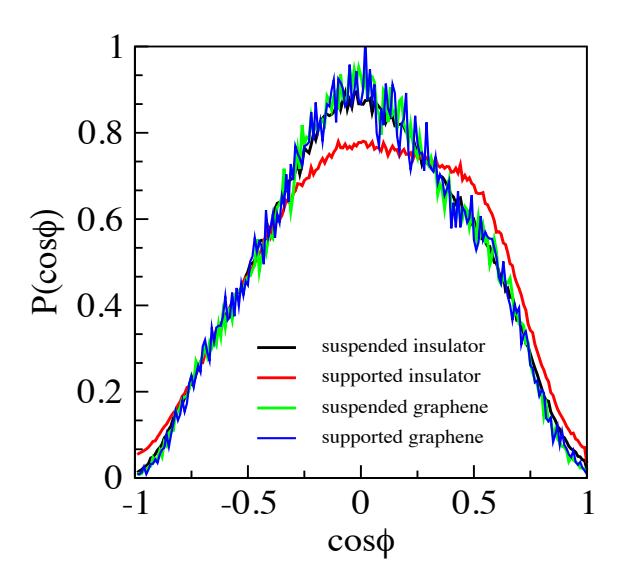


Figure 5: Dipole angle probability distributions  $P(\cos\phi)$  for water molecules in the solid/water contact layer of the cylindrical nanodroplet on different surfaces.  $\epsilon_{co} = 0.3913$  kJ mol<sup>-1</sup>,  $\sigma_{co} = 3.19$ Å. Black line: suspended insulator. Red: water-supported insulator. Green color: suspended graphene, blue color: water-supported graphene.

conventional picture observed with the insulator model, where attractions apply to charges of opposite signs. In addition to the average dipole moments shown in Figure 5, we also calculate the dipole-dipole correlation functions,  $c_{\alpha}(r) = \frac{\langle \delta \mu_{\alpha}^{top}(r) \delta \mu_{\alpha}^{bottom}(0) \rangle}{\langle \delta \mu_{\alpha}^{2} \rangle}$  based on molecular

orientations in the 1<sup>st</sup> hydration layers of the cylindrical droplet base on top of the graphene,  $\mu$ top, and in the aqueous slab below the water-supported sheet,  $\mu$  bottom. To enable the assessment of the absolute magnitudes of  $c_{\alpha}(r)$ , Table 2 presents the variances of dipole components, <  $\delta\mu_{\alpha}^2$  >, which we used to normalize  $c_{\alpha}(r)$ . The calculation of dipole correlation functions is included to highlight a qualitative change of dipolar interactions due to the polarization of conducting graphene layer. We therefore present the results for both the conducting and nonconducting graphene models (Figure 6). The distance r corresponds to the lateral distance between the centers of a pair of dipoles in the opposite hydration layers and the average is taken over all possible pairs. In all cases, the variances  $<\delta\mu_{\alpha}^2>$  are essentially identical on both sides of the sheet. As expected, the correlations across nonconducting graphene sheet at small lateral distances r (Figure 6) are positive for z components (normal to the surface) of the dipole moments of water, and negative for the lateral  $(x \ or \ y)$  components. The signs of  $c_z(r)$  and  $c_{xy}(r)$  at small rare compatible with (average) attraction among the dipoles. Interestingly, the signs of both functions are reversed and the average dipole interactions become weakly repulsive when we apply the conducting graphene model. As such, the *direct* dipole-dipole term does not contribute to the contact angle reduction in the latter system. The sign change is explained in terms of the polarization of graphene, with image charges inside the conductor layer attracting equally signed partial charges of water molecules on both sides of the sheet. Water-graphene attraction is strengthened through enhanced polarization of graphene flanked by equally-signed partial charges facing each other across the sheet thus increasing the wetting propensity (lower contact angle) when water is present on both sides of the conducting graphene layer. We quantify the polarization enhancement on submerged graphene by comparing the induced-charge probabilities on carbon atoms in suspended (one-side wetting) and submerged (both side wetting) graphene sheets. As shown in Fig. 7, the presence of polar water molecules on both sides of the sheet results in a noticeable broadening of the charge distribution. Coulombic dipole/inducedcharge interactions corresponding to representative charge magnitudes (Fig. 7) appear compatible with the estimated induction energy discussed above.

A sign reversal of Coulombic interactions analogous to the one discussed above has been indicated in two<sup>18</sup> and three-dimensional<sup>70,71</sup> ionic systems in the presence of temporal or spatial fluctuations of charge-density distributions. The insulator model devoid of polarization effects, on the other hand, features the expected Coulombic attraction between the partial charges of

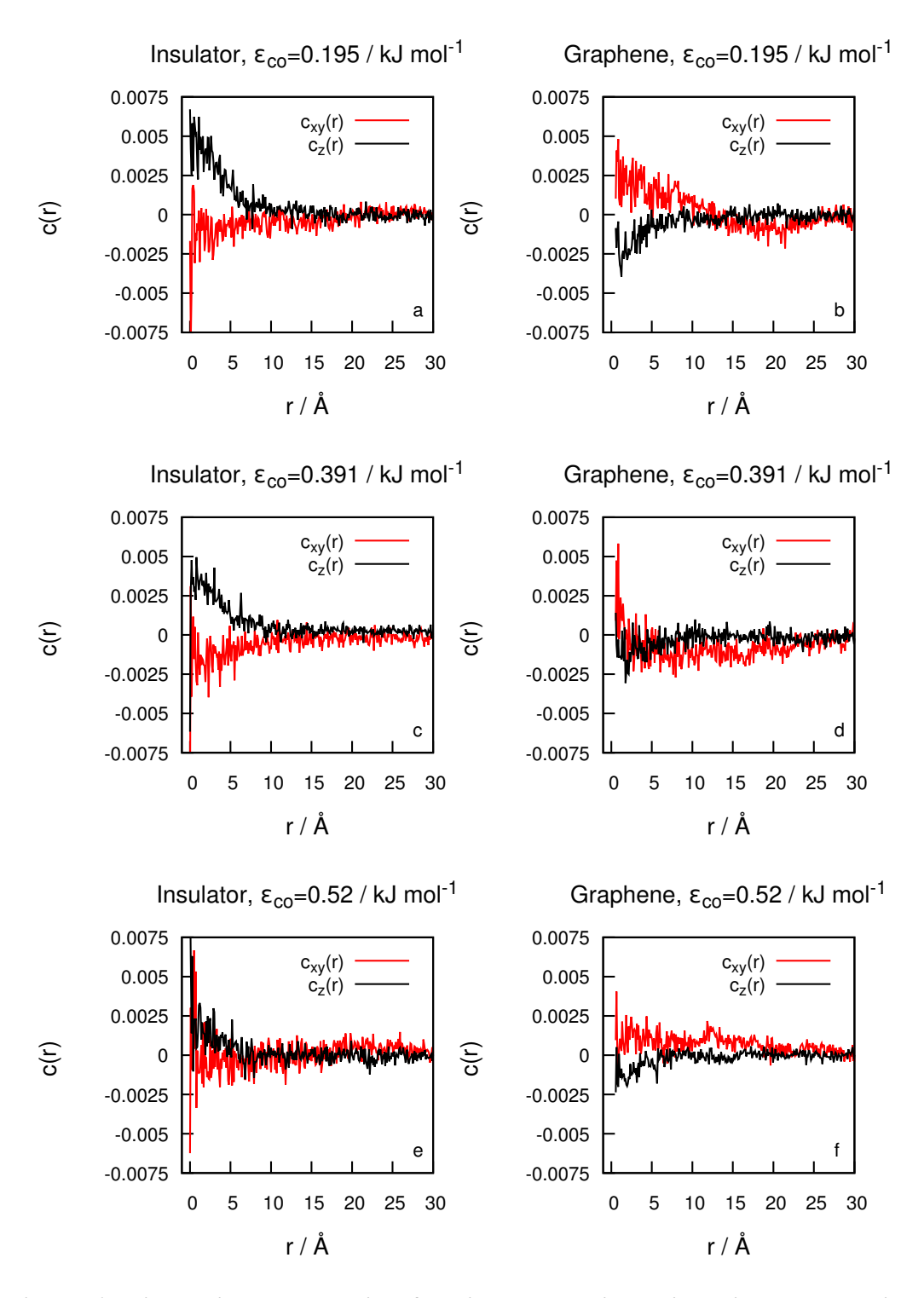


Figure 6: Dipole-dipole correlation functions measuring orientational correlations between water molecules in the hydration layers of a cylindrical droplet atop the insulator sheet (left: a,c,e) or conducting graphene (right: b,d,f), and liquid water below the sheet for different values of  $\varepsilon_{co}$ =0.1951 kJ mol<sup>-1</sup> (top), 0.3913 kJ mol<sup>-1</sup> (middle), and 0.5208 kJ mol<sup>-1</sup> (bottom).  $\sigma_{co}$  = 3.19Å.

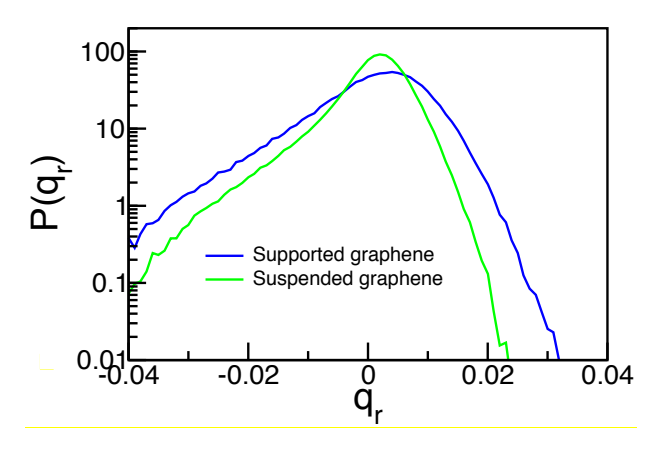
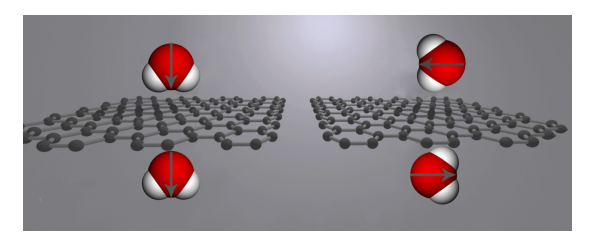


Figure 7: Normalized induced-charge probability densities on carbon atoms below a cylindrical aqueous drop on suspended (green) or supported graphene (blue) sheet with LJ parameters  $\epsilon_{co}=0.3913$  kJ mol $^{-1}$ ,  $\sigma_{co}=3.19$ Å.  $q_r=q$  e $_o^{-1}$ .

opposite signs. Fig. 8 illustrates the (weekly) preferred configurations for a pair of water molecules interacting across the graphene sheet in the presence (right) or absence (left) of graphene polarization. Fig. 8 right also shows positive (blue) and negative charges on carbon atoms induced by the electric field of adjacent water molecules. Induced charges are described by a Gaussian distribution around carbon atoms (width below 1 Å).<sup>52</sup> Charge probabilities for this scenario are described by the blue curve in Fig. 7.

The correlations across the sheet introduce a subtle interaction term, which is superimposed to much stronger molecular interactions (including hydrogen bonding) inside a contiguous liquid on either side of graphene, along with the dispersion attraction to the carbon sheet. These interactions result in a spontaneous near-parallel alignment of the dipoles in the hydration layer along the surface, with only a slight preference for dipole orientation pointing into the liquid phase (See Fig. 8 and Table 2). When water is present on *both* sides of the (nonpolarizable) insulator sheet, the lateral alignment of the dipoles with the surface is slightly



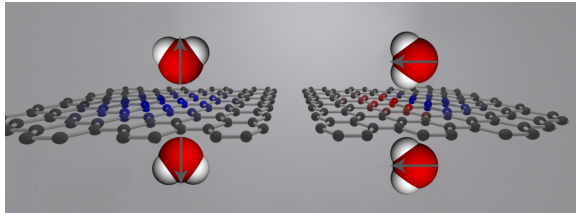


Figure 8: Favored configurations for a pair of water molecules interacting across a graphene sheet submerged under water. Left: insulator sheet, right: conducting graphene. Neutral carbon atoms are shown in grey, whereas we use blue or red color when the atoms carry positive or negative induced charges, respectively.

destabilized (Fig. 5) as the chain dipole-dipole configuration enables a stronger dipolar interaction across the sheet than the antiparallel one.<sup>72</sup> An analogous perturbation of water-wall orientations does not take place with the conducting graphene, where the direct dipole-dipole interaction across the sheet is overwhelmed by the interaction with image charges induced by the molecules from *both* sides of the sheet and where the attraction by the image charges is compatible with the (already favored) lateral dipole alignment with the surface.

Although the conducting graphene screens the direct interaction between the dipoles on the opposing sides of graphene, the attraction by image charges induced by the molecules from both sides results in the overall *increase* in the wetting affinity and a reduction of the contact angle relative to that observed with the insulator model. Interestingly, the synergistic effect of graphene polarization due to the molecules from both sides is required to observe a notable contact angle change, while the introduction of material's conductivity has a smaller effect with droplets on suspended graphene, *i.e.* in the absence of aqueous support.

To illustrate the conductivity and hydrophilicity effects on spontaneous orientation and orientational polarizability, in Table 2 we compare the average dipole moment normal to the graphene surface and the variance of the normal and lateral dipole components for both nonconducting and conducting graphene characterized by different water-carbon interaction strengths from Table 1. The weak polarization of water quantified in terms of finite  $<\mu_z>$  (with the dipoles pointing slightly away from the interface) slowly increases upon strengthening the water-surface attraction. The change takes place symmetrically on both sides of the sheet, however, the statistical quality of calculated  $<\mu_z>$  is better in the water slab below the sheet  $(<\mu_z>_{bot})$  than in the hydration layer of the droplet base  $(<\mu_z>_{top})$  where the results may be affected by the fluctuations of the drop's perimeter. While the addition of water on both sides of the insulating sheet weakens the preference for the dipole alignment with the surface (Figure 5), the positive and negative deviations mostly cancel, leaving only a small enhancement of the polarization  $<\mu_z>$  upon the introduction of aqueous support under graphene.

The data describing orientation fluctuations of water molecules next to graphene (Table 2) show a significant difference between the variances of water dipole components in the normal and lateral directions. The difference conforms to the known<sup>73</sup> anisotropies of the orientational polarizability and permittivity tensors of interfacial water. Specifically, the orientational

polarizability of water molecules along the surface normal,  $\alpha_{zz}^{or} \sim \frac{\langle \delta \mu_z^2 \rangle}{kT}$ , is almost twice smaller than the corresponding values in the lateral (x,y) directions.  $\alpha_{zz}^{or}$  decreases further with strengthened orientational restrictions when the surface is rendered more hydrophilic. A similar effect is observed in the presence of image charges in graphene when treated as a conductor. Conversely, the increase in hydrophilicity, and the addition of image charge effects, result in a slight *enhancement* of the lateral polarizability components  $(\alpha_{xx}^{or}$  and  $\alpha_{yy}^{or})$ . Because of the close relation between the dielectric constant and the dipoles' fluctuation  $\langle \delta \mu \rangle^2$ , our results indicate that the lateral components of the permittivity tensor substantially exceed the normal component in analogy to the observations in a planar confinement.<sup>74</sup>

Table 2: Average dipole moments (in D) and mean squared fluctuations of dipole components (x, y, or z) of water molecules in the first hydration layers of an insulating (a) and conducting (b) model graphene sheets wetted by an aqueous drop on the top side and supported by an aqueous slab on the bottom, all for three different carbon-water interaction strengths  $\varepsilon_{co}$ . (c) suspended insulating sheet.

# (a) graphene-like insulator sheet on water

$\frac{\varepsilon_{co}}{1111111111111111111111111111111111$	$<\mu_z>_{top}$	$<\mu_z>_{bot}$	$<\delta\mu_{x,y}^2>$	$<\delta\mu_{z}^{2}>$
kJmol⁻¹	D	D	$D^2$	$D^2$
0.1951	0.100±3%	-0.110±1%	2.19±0.5%	1.14±0.5%
0.3913	0.124±3%	-0.122±1%	2.21±0.5%	1.08±0.5%
0.5208	0.132±3%	-0.128±1%	2.23±0.5%	1.04±0.5%

## (b) conducting graphene on water

$\frac{\mathcal{E}_{co}}{1.1 - 1}$	$<\mu_z>_{top}$	$<\mu_{\rm z}>_{\rm bot}$	$<\delta\mu_{x,y}^2>$	$<\delta\mu_{\rm z}^2>$
kJmol⁻¹	D	D	$D^2$	$D^2$
0.1951	0.104±3%	-0.104±1%	2.20±0.5%	1.10±0.5%
0.3913	0.120±3%	-0.122±1%	2.24±0.5%	1.04±0.5%
0.5208	0.126±3%	-0.134±1%	2.26±0.5%	0.99±0.5%

# (c) suspended sheet:

$\frac{\varepsilon_{\rm co}}{kJmol^{-1}}$	$<\mu_{\rm z}>_{insulator}^{top}$	$<\mu_{\rm z}>_{graphene}^{top}$
0.1951	0.089±3%	0.106±3%
0.3913	0.122±3%	0.129±3%
0.5208	0.130±3%	0.133±3%

**Non-Polar Liquid.** To enable a comparison with systems devoid of long-range electrostatics, we follow the same procedure to compute contact angles of diiodomethane ( $CH_2I_2$ ) on suspended and  $CH_2I_2$ - supported graphene sheets. The hemicylindrical drop was divided into three slices to remove the possible effect due to long-range triple line fluctuations. The drop contour of each slice was calculated through a square binning of the local number of heavy (C and C) atoms on the yz plane with a C4 resolution.

The results for time-averaged contact angles of diiodomethane on suspended and supported graphene are 50.8° and 48.9°, respectively. The contact angle reduction of about 2° affirms a degree of 'wetting translucency' when the liquid molecules interact across graphene solely through dispersion forces. Within statistical uncertainty, the magnitude of the effect agrees with the mean field prediction for the van der Waals contribution to the contact angle reduction:

$$\Delta\cos\theta \sim = -\frac{2\pi\sum_{i}\sum_{j}\rho_{i}\rho_{j}}{6\gamma}\frac{\varepsilon_{ij}\sigma_{ij}^{6}}{d_{ii}^{2}}$$

$$\tag{4}$$

introduced in our earlier work<sup>35</sup>. Here, the summation runs over all interacting site pairs (i,j) of liquid molecules (I and CH<sub>2</sub> with the united-atom CH<sub>2</sub>I<sub>2</sub> model) of site number densities  $\rho_i$  and Lennard Jones parameters  $\varepsilon_{ij} = (\varepsilon_i \varepsilon_j)^{1/2}$ ,  $\sigma_{ij} = (\sigma_{i} + \sigma_{j})/2$ , and  $d_{ij} = (\sigma_{c} + \sigma_{ij})$ .  $\gamma$  is the surface tension of the liquid. Using the diiodomethane parameters collected in the Force fields section obtains the contact angle reduction for the submerged graphene in diiodomethane  $\Delta\theta \sim -3^{\circ}$ . Since diiodomethane molecules carry only minute atom charges (see Methods section), the electrostatic interactions between the droplet and the solvent slab below graphene, along with any image charge effects, remain too weak to manifest the trends observed with the highly polar water molecules (Fig. 6). The results for the diiodomethane system are hence independent of whether we treat graphene as an insulator or a conductor; the use of the advanced CAPMD approach is not warranted in these cases.

### **CONCLUSIONS**

Using Constant Applied Potential Molecular Dynamics simulations, we examine the influence of liquid-liquid interactions across a *conducting* graphene sheet on the wetting propensity, which we quantify in terms of the contact angle of a cylindrical nanodroplet spreading over the graphene surface. We present a comparison between the systems with and

without the supporting liquid under the sheet, and with systems ignoring graphene's conductivity and associated polarization. Our results show the impact of the supporting liquid is substantially stronger when graphene's conductivity is taken into account notwithstanding the screening of direct electrostatic interactions between polar molecules at the opposite sides of the graphene layer. We explain this counterintuitive behavior in terms of the effective attraction between partial molecular charges of the equal sign, mediated by image charges induced in graphene to eliminate the lateral electric field inside the conductor. The mechanism is confirmed by monitoring the orientational correlations among water molecules at the opposite sides of the graphene sheet. A pair of water molecules facing each other across an insulator sheet tend to favor an antiparallel alignment along lateral (x,y) directions and a parallel one along the surface normal (z) to minimize their dipolar interaction. Addition of water under graphene sheet hence perturbs molecular orientations in the droplet base atop the sheet. When we incorporate graphene conductivity, the polarization of the model graphene sheet shields the direct dipole-dipole interactions across it. The image charges on graphene, positioned between the partial charges on water atoms at the opposite sides of the sheet introduce an indirect attraction between like charges, reversing the sign of dipolar correlations across the sheet. To balance the electrostatic potential due to like charges of polar water molecules from both sides of the sheet enhances the magnitude of local graphene polarization, resulting in an enhanced propensity for wetting. The reduction of water contact angle on the conducting graphene wetted on both sides is hence considerably greater than predicted using the insulator graphene model. Accounting for this difference is significant for accurate model predictions of wetting properties of graphene on the one hand, or related dielectric materials like e.g. boron-nitride, 61 phosphorene, 75 or saturated derivatives of graphene on the other. The self-consistent atomic polarization model of ref.<sup>39</sup> can also describe induction effects in the latter class of 2-dimensional materials. Parallel computations in a nonpolar liquid, diiodomethane, whose properties are dominated by the van der Waals interactions, on the other hand, show no dependence on graphene electrostatics. In this case, a moderate wettability increase upon two-side wetting agrees with the mean field prediction for the contact angle reduction, which relies solely on direct dispersion forces between the liquid molecules on two sides of the sheet, unaffected by the intervening carbon layer.

### MODELS AND METHODS

Force fields: The nonconducting model surface consists of a single layer of 5600 charge-free carbon atoms on graphene lattice, interacting with water *via* the Lennard-Jones (LJ) potential.<sup>35, 76,77</sup> The conductor behavior of graphene is captured by the addition of fluctuating Gaussian charges on carbon atoms as outlined in the Discussion section. We mitigate finite size effects by periodically replicating the surface in the lateral (*x,y*) directions. While the addition of local defects, impurities, and surface corrugations greatly enrich the physics of graphene-based materials, in the present work we only consider neat, ideally smooth graphene surfaces. Neglecting the surface flexibility, <sup>78</sup> graphene atom positions are held fixed during the simulation. Clearly, the CAPMD approach becomes inaccurate and eventually breaks down with increasing deformations <sup>79</sup> or chemical modifications <sup>80</sup> conducive to band gap opening and a concomitant transition to the semiconductor or insulator behavior. It is unclear what extent of corrugation would be required to observe an appreciable reduction of the screening effectiveness of the sheet in the present context.

We use identical graphene surface in simulations of aqueous and diiodomethane droplets. Following the preceding work,<sup>35</sup> we described water interactions by the extended simple point charge potential (SPC/E)<sup>63, 81</sup> which has been known to capture the essential interfacial and dielectric properties of liquid water. The use of this force field is motivated by our recent dynamic studies of bulk and confined water.<sup>33, 76, 82,87</sup> The potential consists of a Coulomb potential acting between partial point charges on oxygen ( $-0.8476~e_0$ ) and hydrogen ( $0.4238~e_0$ ) atoms with O-H distance 1Å and H-O-H angle at 109.47°. The oxygen atoms also interact *via* LJ potential with  $\varepsilon_{00}$ =0.651 kJ mol<sup>-1</sup> and  $\sigma_{00}$ =3.166 Å. The LJ interaction between the SPC/E water molecules and carbon atoms on graphene is characterized by  $\varepsilon_{co}$  values from 0.19 to 0.51 kJ mol<sup>-1</sup> and we use a smooth LJ cutoff at 12 Å. The carbon atom LJ diameter  $\sigma_{cc}$  = 3.214 Å leads to the water-carbon contact distance  $\sigma_{co}$  = 3.19 Å.

The non-polar droplet is comprised of 850 diiodomethane,  $CH_2I_2$ , molecules with the CH<sub>2</sub> group modeled using the united atom representation. The united atom CH<sub>2</sub> group carries a charge  $0.022e_0$  and each of the explicit I atoms has a point charge  $-0.011e_0$ . The I-CH2 bond length is 2.21 Å and the I-CH<sub>2</sub> -I bond angle is  $116.6^{\circ}$ . We use the LJ potentials corresponding

to  $\varepsilon_{CH_2} = 0.4105 kJ \ mol^{-1}$ ,  $\varepsilon_I = 3.5 \ kJ \ mol^{-1}$ ,  $\sigma_{CH_2} = 4.07 \ \text{Å}$ ,  $\sigma_I = 3.849 \ \text{Å}^{88,89}$  with the Lorentz-Berthelot mixing rules and the LJ cutoff distance of 12 Å.

Molecular dynamics. In the absence of material's conductivity, the simulations were performed using the large-scale atomic molecular massively parallel simulator package (LAMMPS).<sup>90</sup> The temperature was held constant at 300K using the Nose-Hoover thermostat<sup>91</sup> with a relaxation time of 0.2ps. Verlet integration was used with time step 2 fs. The total length of a typical run was 3ns. Long-range electrostatic interactions were computed using the particle-particle-particle-mesh (PPPM) solver, with 10<sup>-5</sup> accuracy. The slab correction of Yeh and Berkowitz<sup>92</sup> was added to the Ewald summation to account for the two-dimensional periodicity of our system. The computations for conducting graphene were performed using an adaptation<sup>86</sup> of the Constant Applied Potential MD (CAPMD)<sup>52</sup> code designed for simulations of two-electrode systems with a preset interelectrode potential difference.<sup>93</sup> The lateral periodicity was enforced by rigorous two-dimensional Ewald summation.<sup>52</sup> To enable the use of the original CAPMD code designed to control the difference between separate conducting objects, we treated the model graphene plate as a pair of distinct 'electrodes' at identical potential by assigning a vanishing V<sub>i</sub><sup>0</sup> to all carbon atoms j (denoted by different colors in Fig. 1d).

Simulation details. The simulations start by placing a water droplet on a rectangular lattice containing  $\sim 6.4 \times 10^3$  water molecules on the graphene surface. The surface of size  $123\text{\AA} \times 119\text{\AA}$  coincides with the (x,y) plane. The initial drop has a quadratic cross-section in (x,z) plane and extends along the entire surface width along the x direction. During the equilibration, the droplet acquires a cylindrical shape illustrated in Figure 1. Our choice to employ cylindrical rather than hemispherical drop has been motivated by two reasons. The cylindrical droplet avoids the curvature of the three-phase contact line, which leads to considerable line tension effects with hemispherical nanodroplets. An additional advantage of the semi-infinite cylindrical geometry is the optimization of parallelized computation. The improved computational efficiency permits simulation of bigger cylindrical drops compared to calculations in the hemispherical drop geometry, improving the statistics of contact angle calculation.

All MD simulations were initialized by using the LAMMPS package. Since LAMMPS is orders of magnitude faster than CAPMD code,  $^{52}$ ,  $^{86}$  it enabled an efficient pre-equilibration before running the CAPMD simulations. While we performed NVT molecular dynamics simulations, the system maintained a droplet-vapor equilibrium with pressure fluctuating around the vapor pressure of the liquid. The two types of systems we considered comprised a cylindrical drop on the suspended model graphene surface or the surface supported by a uniform liquid of slab thickness around  $13.1\,\text{Å}$  which contains  $\sim 6.9 \times 10^3$  water molecules or 2000 diiodomethanes. The above width has been demonstrated sufficient to secure the convergence of the droplet properties atop the graphene layer with respect to the dimensions of the supporting liquid slab. In order to keep the slab thickness uniform, below the slab we introduced an implicit wall interacting with the liquid molecules through a harmonic repulsion. A second wall is also placed at the top boundary of the simulation box to prevent the escape of vapor water molecules along the non-periodic z direction. The details of auxiliary walls placement and the repulsive potential bear no effect on the calculated wetting behavior on graphene.

Contact angle measurement. To establish a direct connection with experiments, 25,26,31,36 we determine the microscopic analogue of the droplet contact angle. We use a technique<sup>33</sup> similar to that presented by de Ruijter et al. 95 that characterizes the dynamics of droplet spreading by calculating the dynamic contact angle for each configuration. We divide the hemicylindrical drop to three slices to remove the possible effect due to long-range triple line fluctuation. The contour of each slice is calculated through a square binning of the local density of water on the yz plane with a 2Å resolution. The dividing surface corresponds to the iso-density plane with half the density of the droplet core. The contact angle is determined from the circular fit of the drop contour. 96 Because of the known droplet distortion within a few molecular diameters from the solid surface, we fit only the contour above the heights characterized by detectable liquid/solid density profile oscillatons. 95, 97 We adopt the empirical threshold height at half the oscillation period above the second density peak. In view of worsened statistics near the top of the drop, we determine the drop contour from the computed density distributions within ~10 Å thick midsection of the drop, parallel to the x direction and centered with respect to the drop center of mass.<sup>33</sup> The contact angle is determined at the cross-section of the contour and the reference contact plane at an oxygen radius below the first liquid density peak.

#### **ACKNOWLEDGMENTS**

While performing this work, D. B. was supported by the Office of Basic Energy Sciences, Chemical Sciences, Geosciences, and Biosciences Division of the U.S. Department of Energy (Grant No. DE-SC 0004406) and N.O. and A.L. were supported by the National Science Foundation under Grant No. CHE-1800120. We acknowledge the supercomputer time from Extreme Science and Engineering Discovery Environment (XSEDE), supported by NSF Grant No. OCI-1053575, and the National Energy Research Scientific Computing Center (NERSC), supported by the Office of Science of the U.S. Department of Energy (No. DEAC02-05CH11231).

#### REFERENCES

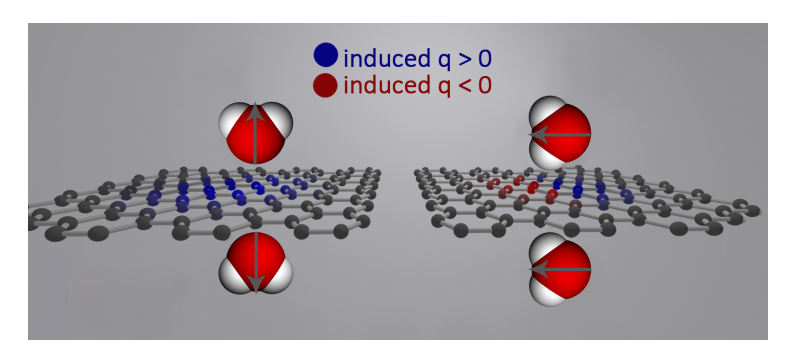
- 1. Geim, A. K. Graphene: Status and Prospects. *Science* **2009**, *324*, 1530-1534.
- 2. Zhong, Y. J.; Zhen, Z.; Zhu, H. W. Graphene: Fundamental Research and Potential Applications. *Flatchem* **2017**, *4*, 20-32.
- 3. Abergel, D. S. L.; Apalkov, V.; Berashevich, J.; Ziegler, K.; Chakraborty, T. Properties of Graphene: A Theoretical Perspective. *Adv. Phys.* **2010**, *59*, 261-482.
- 4. Sattar, T. Current Review on Synthesis, Composites and Multifunctional Properties of Graphene. *Top. Curr. Chem.* **2019**, *377*, 10.
- 5. Osada, M.; Sasaki, T. Two-Dimensional Dielectric Nanosheets: Novel Nanoelectronics from Nanocrystal Building Blocks. *Adv. Mater.* **2012**, *24*, 210-228.
- 6. Nandee, R.; Chowdhury, M. A.; Ahmed, M. U.; Shuvho, B. A.; Debnath, U. K. Performance and Characterization of Two-Dimensional Material Graphene Conductivity-a Review. *Mater. Performance Charact.* **2019**, *8*, 183-196.
- 7. Ferrari, G. A.; de Oliveira, A. B.; Silvestre, L.; Matos, M. J. S.; Batista, R. J. C.; Fernandes, T. F. D.; Meireles, L. M.; Eliel, G. S. N.; Chacham, H.; Neves, B. R. A.; Lacerda, R. G. Apparent Softening of Wet Graphene Membranes on a Microfluidic Platform. *ACS Nano* **2018**, *12*, 4312-4320.
- 8. Liu, F. Y.; Navaraj, W. T.; Yogeswaran, N.; Gregory, D. H.; Dahiya, R. Van Der Waals Contact Engineering of Graphene Field-Effect Transistors for Large-Area Flexible Electronics. *ACS Nano* **2019**, *13*, 3257-3268.
- 9. Mas-Balleste, R.; Gomez-Navarro, C.; Gomez-Herrero, J.; Zamora, F. 2D Materials: To Graphene and Beyond. *Nanoscale* **2011**, *3*, 20-30.
- 10. Fiori, G.; Bonaccorso, F.; Iannaccone, G.; Palacios, T.; Neumaier, D.; Seabaugh, A.; Banerjee, S. K.; Colombo, L. Electronics Based on Two-Dimensional Materials. *Nat. Nanotechnol.* **2014**, *9*, 768-779.
- 11. Yazyev, O. V.; Chen, Y. P. Polycrystalline Graphene and Other Two-Dimensional Materials. *Nat. Nanotechnol.* **2014**, *9*, 755-767.
- 12. Zhang, G. Y.; Du, S. X.; Wu, K. H.; Gao, H. J. Two-Dimensional Materials Research. *Science* **2018**, *360*, 15-18.
- 13. Zhang, H. Ultrathin Two-Dimensional Nanomaterials. *ACS Nano* **2015**, *9*, 9451-9469.
- 14. Pan, J.; Lany, S.; Qi, Y. Computationally Driven Two-Dimensional Materials Design: What Is Next? *ACS Nano* **2017**, *11*, 7560-7564.
- 15. Qiu, L.; Li, D.; Cheng, H. M. Structural Control of Graphene-Based Materials for Unprecedented Performance. *ACS Nano* **2018**, *12*, 5085-5092.
- 16. Abdelmoaty, Y. H.; Tessema, T. D.; Norouzi, N.; El-Kadri, O. M.; Turner, J. B. M.; E-Kaderi, H. M. Effective Approach for Increasing the Heteroatom Doping Levels of Porous Carbons for Superior Co<sub>2</sub> Capture and Separation Performance. *ACS Appl. Mat. Interfaces* **2017**, *9*, 35802-35810.

- 17. Pykal, M.; Langer, M.; Prudilova, B. B.; Banas, P.; Otyepka, M. Ion Interactions across Graphene in Electrolyte Aqueous Solutions. *J. Phys. Chem. C* **2019**, *123*, 9799-9806.
- 18. Mendez-Morales, T.; Burbano, M.; Haefele, M.; Rotenberg, B.; Salanne, M. Ion-Ion Correlations across and between Electrified Graphene Layers. *J. Chem. Phys.* **2018**, *148*, 193812.
- 19. Lu, Y.; Yang, F.; Wang, G. G. X.; Zhang, T. Y.; Wang, P. Recent Development of Graphene-Based Materials for Cathode Application in Lithium Batteries: A Review and Outlook. *Int. J. Appl. Electrochem. Sci.* **2019**, *14*, 5961-5971.
- 20. Al Hassan, M. R.; Sen, A.; Zaman, T.; Mostari, M. S. Emergence of Graphene as a Promising Anode Material for Rechargeable Batteries: A Review. *Mater. Yoday. Chem.* **2019**, *11*, 225-243.
- 21. Wang, W. R.; Su, H. J.; Wu, Y. X.; Zhou, T.; Li, T. Review-Biosensing and Biomedical Applications of Graphene: A Review of Current Progress and Future Prospect. *J. Electrochem. Soc.* **2019**, *166*, B505-B520.
- 22. Andrews, J. E.; Sinha, S.; Chung, P. W.; Das, S. Wetting Dynamics of a Water Nanodrop on Graphene. *Phys. Chem. Chem. Phys.* **2016**, *18*, 23482-23493.
- 23. Gim, S.; Lim, H. K.; Kim, H. Multiscale Simulation Method for Quantitative Prediction of Surface Wettability at the Atomistic Level. *J. Phys. Chem. Lett.* **2018**, *9*, 1750-1758.
- 24. Diao, Y. J.; Greenwood, G.; Wang, M. C.; Nam, S.; Espinosa-Marzal, R. M. Slippery and Sticky Graphene in Water. *ACS Nano* **2019**, *13*, 2072-2082.
- 25. Hong, G.; Han, Y.; Schutzius, T. M.; Wang, Y. M.; Pan, Y.; Hu, M.; Jie, J. S.; Sharma, C. S.; Muller, U.; Poulikakos, D. On the Mechanism of Hydrophilicity of Graphene. *Nano Lett.* **2016**, *16*, 4447-4453.
- 26. Feng, J.; Guo, Z. G. Wettability of Graphene: From Influencing Factors and Reversible Conversions to Potential Applications. *Nanoscale Horizons* **2019**, *4*, 339-364.
- 27. Melios, C.; Giusca, C. E.; Panchal, V.; Kazakova, O. Water on Graphene: Review of Recent Progress. 2d Materials 2018, 5, 022001.
- 28. Li, H.; Zeng, X. C. Wetting and Interfacial Properties of Water Nanodroplets in Contact with Graphene and Monolayer Boron-Nitride Sheets. *ACS Nano* **2012**, *6*, 2401-2409.
- 29. Rafiee, J.; Mi, X.; Gullapalli, H.; Thomas, A. V.; Yavari, F.; Shi, Y. F.; Ajayan, P. M.; Koratkar, N. A. Wetting Transparency of Graphene. *Nat. Mater.* **2012**, *11*, 217-222.
- 30. Shih, C. J.; Wang, Q. H.; Lin, S. C.; Park, K. C.; Jin, Z.; Strano, M. S.; Blankschtein, D. Breakdown in the Wetting Transparency of Graphene. *Phys. Rev. Lett.* **2012**, *109*, 049901.
- 31. Kim, D.; Pugno, N. M.; Buehler, M. J.; Ryu, S. Solving the Controversy on the Wetting Transparency of Graphene. *Sci. Rep.* **2015**, *5*, 15526.
- 32. Ondarcuhu, T.; Thomas, V.; Nunez, M.; Dujardin, E.; Rahman, A.; Black, C. T.; Checco, A. Wettability of Partially Suspended Graphene. *Sci. Rep.* **2016**, *6*, 24237.
- 33. Vanzo, D.; Bratko, D.; Luzar, A. Wettability of Pristine and Alkyl-Functionalized Graphane. *J. Chem. Phys.* **2012**, *137*, 034707.
- 34. Li, Z. T.; Wang, Y. J.; Kozbial, A.; Shenoy, G.; Zhou, F.; McGinley, R.; Ireland, P.; Morganstein, B.; Kunkel, A.; Surwade, S. P.; Li, L.; Liu, H. T. Effect of Airborne Contaminants on the Wettability of Supported Graphene and Graphite. *Nat. Mater.* **2013**, *12*, 925-931.
- 35. Driskill, J.; Vanzo, D.; Bratko, D.; Luzar, A. Wetting Transparency of Graphene in Water. *J. Chem. Phys.* **2014**, *141*, 18C517.
- 36. Belyaeva, L. A.; van Deursen, P. M. G.; Barbetsea, K. I.; Schneider, G. F. Hydrophilicity of Graphene in Water through Transparency to Polar and Dispersive Interactions. *Adv. Mater.* **2018**, *30*, 1703274.
- 37. Bormashenko, E. Progress in Understanding Wetting Transitions on Rough Surfaces. *Adv. Colloid. Interface Sci.* **2015**, 222, 92-103.
- 38. Ho, T. A.; Striolo, A. Polarizability Effects in Molecular Dynamics Simulations of the Graphene-Water Interface. *J. Chem. Phys.* **2013**, *138*, 054117
- 39. Misra, R. P.; Blankschtein, D. Insights on the Role of Many-Body Polarization Effects in the Wetting of Graphitic Surfaces by Water. *J. Phys. Chem. C* **2017**, *121*, 28166-28179.

- 40. Williams, C. D.; Dix, J.; Troisi, A.; Carbone, P. Effective Polarization in Pairwise Potentials at the Graphene-Electrolyte Interface. *J. Phys, Chem. Lett.* **2017**, *8*, 703-708.
- 41. Liu, J.; Lai, C. Y.; Zhang, Y. Y.; Chiesa, M.; Pantelides, S. T. Water Wettability of Graphene: Interplay between the Interfacial Water Structure and the Electronic Structure. *Rsc Advances* **2018**, *8*, 16918-16926.
- 42. Walther, J. H.; Werder, T.; Jaffe, R. L.; Gonnet, P.; Bergdorf, M.; Zimmerli, U.; Koumoutsakos, P. Water-Carbon Interactions Iii: The Influence of Surface and Fluid Impurities. *Phys. Chem. Chem. Phys.* **2004**, *6*, 1988-1995.
- 43. Yu, E. K.; Stewart, D. A.; Tiwari, S. *Ab Initio* Study of Polarizability and Induced Charge Densities in Multilayer Graphene Films. *Phys. Rev. B* **2008**, 77, 195406.
- 44. Santos, E. J. G.; Kaxiras, E. Electric-Field Dependence of the Effective Dielectric Constant in Graphene. *Nano Lett.* **2013**, *13*, 898-902.
- 45. Du, F.; Huang, J. Y.; Duan, H. L.; Xiong, C. Y.; Wang, J. X. Wetting Transparency of Supported Graphene Is Regulated by Polarities of Liquids and Substrates. *Appl. Surface Sci.* **2018**, *454*, 249-255.
- 46. Kong, W.; Li, H. S.; Qiao, K.; Kim, Y.; Lee, K.; Nie, Y. F.; Lee, D.; Osadchy, T.; Molnar, R. J.; Gaskill, D. K.; Myers-Ward, R. L.; Daniels, K. M.; Zhang, Y. W.; Sundram, S.; Yu, Y.; Bae, S. H.; Rajan, S.; Shao-Horn, Y.; Cho, K.; Ougazzaden, A.; Grossman, J. C.; Kim, J. Polarity Governs Atomic Interaction through Two-Dimensional Materials. *Nat. Mater.* **2018**, *17*, 999-+.
- 47. Schyman, P.; Jorgensen, W. L. Exploring Adsorption of Water and Ions on Carbon Surfaces Using a Polarizable Force Field. *J. Phys. Chem. Lett.* **2013**, *4*, 468-474.
- 48. Sharma, J. D.; Sharma, M.; Kumar, N.; Ahluwalia, P. K.; Iop, Computational Study of Dielectric Function and Optical Properties of a Graphane Nano Structure Containing Graphene Quantum Dot. In *Dielectrics*, 2013; Vol. 472, p 012010.
- 49. Yang, J. Y.; Liu, L. H. Effects of Interlayer Screening and Temperature on Dielectric Functions of Graphene by First-Principles. *J. Appl. Phys.* **2016**, *120*, 034305.
- 50. Kozinsky, B.; Marzari, N. Static Dielectric Properties of Carbon Nanotubes from First Principles. *Phys. Rev. Lett.* **2006**, *96*.
- 51. Siepmann, J. I.; Sprik, M. Influence of Surface-Topology and Electrostatic Potential on Water Electrode Systems. *J. Chem. Phys.* **1995**, *102*, 511-524.
- 52. Reed, S. K.; Lanning, O. J.; Madden, P. A. Electrochemical Interface between an Ionic Liquid and a Model Metallic Electrode. *J. Chem. Phys.* **2007**, *126*, 084704.
- 53. Geissler, P. L.; Dellago, C.; Chandler, D.; Hutter, J.; Parrinello, M. Autoionization in Liquid Water. *Science* **2001**, *291*, 2121-2124.
- 54. Eaves, J. D.; Tomakoff, A. Electric Field Fluctuations Drive Vibrational Dephasing in Water. *J. Phys. Chem. A* **2005**, *109*, 9424-9436.
- 55. Bernholc, J.; Brenner, D.; Nardelli, M. B.; Meunier, V.; Roland, C. Mechanical and Electrical Properties of Nanotubes. *Ann. Rev. Mater. Res.* **2002,** *32*, 347-375.
- 56. Choudhury, N.; Pettitt, B. M. On the Mechanism of Hydrophobic Association of Nanoscopic Solutes. *J. Am. Chem. Soc.* **2005**, *127*, 3556-3567.
- 57. Zangi, R. Are Buckyballs Hydrophobic? *J. Phys. Chem. B* **2014**, *118*, 12263-12270.
- 58. Eun, C.; Berkowitz, M. L. Fluctuations in Number of Water Molecules Confined between Nanoparticles. *J. Phys. Chem. B* **2010**, *114*, 13410-13414.
- 59. Li, L. W.; Bedrov, D.; Smith, G. D. Water-Induced Interactions between Carbon Nanoparticles. *J. Phys. Chem. B* **2006**, *110*, 10509-10513.
- 60. Wang, Z. X.; Yang, Y.; Olmsted, D. L.; Asta, M.; Laird, B. B. Evaluation of the Constant Potential Method in Simulating Electric Double-Layer Capacitors. *J. Chem. Phys.* **2014**, *141*, 184102.
- 61. Kumar, P.; Chauhan, Y. S.; Agarwal, A.; Bhowmick, S. Thickness and Stacking Dependent Polarizability and Dielectric Constant of Graphene-Hexagonal Boron Nitride Composite Stacks. *J. Phys. Chem. C* **2016**, *120*, 17620-17626.
- 62. Phillips, J., Chemical Theory of Bonds and Energy Gaps. In *Covalent Bonding in Crystals*, *Molecules and Polymers*, The University of Chicago Press: Chicago, IL, 1969; pp 125-130.

- 63. Berendsen, H. J. C.; Grigera, J. R.; Straatsma, T. P. The Missing Term in Effective Pair Potentials. *J. Phys. Chem.* **1987**, *91*, 6269-6271.
- 64. Wang, S. R.; Zhang, Y.; Abidi, N.; Cabrales, L. Wettability and Surface Free Energy of Graphene Films. *Langmuir* **2009**, *25*, 11078-11081.
- 65. Zhou, H.; Ganesh, P.; Presser, V.; Wander, M. C. F.; Fenter, P.; Kent, P. R. C.; Jiang, D. E.; Chialvo, A. A.; McDonough, J.; Shuford, K. L.; Gogotsi, Y. Understanding Controls on Interfacial Wetting at Epitaxial Graphene: Experiment and Theory. *Phys. Rev. B* **2012**, *85*, 035406.
- 66. Werder, T.; Walther, J. H.; Jaffe, R. L.; Halicioglu, T.; Koumoutsakos, P. On the Water-Carbon Interaction for Use in Molecular Dynamics Simulations of Graphite and Carbon Nanotubes. *J. Phys. Chem. B* **2003**, *107*, 1345-1352.
- 67. Vega, C.; de Miguel, E. Surface Tension of the Most Popular Models of Water by Using the Test-Area Simulation Method. *J. Chem. Phys.* **2007**, *126*, 154707.
- 68. Leroy, F.; Liu, S. Y.; Zhang, J. G. Parametrizing Nonbonded Interactions from Wetting Experiments *via* the Work of Adhesion: Example of Water on Graphene Surfaces. *J. Phys. Chem. C* **2015**, *119*, 28470-28481.
- 69. Lamoureux, G.; Harder, E.; Vorobyov, I. V.; Roux, B.; MacKerell, A. D. A Polarizable Model of Water for Molecular Dynamics Simulations of Biomolecules. *Chem. Phys. Lett.* **2006**, *418*, 245-249.
- 70. Chakraborty, A. K.; Bratko, D.; Chandler, D. Diffusion of Ionic Penetrants in Charged Disordered Media. *J. Chem. Phys.* **1994**, *100*, 1528-1541.
- 71. Bratko, D.; Chakraborty, A. K. Ion-Ion Correlations in Quenched Disordered Media. *J. Chem. Phys.* **1996**, *104*, 7700-7712.
- 72. Bratko, D.; Striolo, A.; Wu, J. Z.; Blanch, H. W.; Prausnitz, J. M. Orientation-Averaged Pair Potentials between Dipolar Proteins or Colloids. *J. Phys. Chem. B* **2002**, *106*, 2714-2720.
- 73. Matyushov, D. V. Electrostatics of Liquid Interfaces. J. Chem. Phys. 2014, 140, 224506.
- 74. Ballenegger, V.; Hansen, J. P. Dielectric Permittivity Profiles of Confined Polar Fluids. *J. Chem. Phys.* **2005**, *122*, 114711.
- 75. Kumar, P.; Bhadoria, B. S.; Kumar, S.; Bhowmick, S.; Chauhan, Y. S.; Agarwal, A. Thickness and Electric-Field-Dependent Polarizability and Dielectric Constant in Phosphorene. *Phys. Rev. B* **2016**, *93*, 195428.
- 76. Vanzo, D.; Bratko, D.; Luzar, A. Dynamic Control of Nanopore Wetting in Water and Saline Solutions under an Electric Field. *J. Phys. Chem. B* **2015**, *119*, 8890-8899.
- 77. Fang, C.; Wu, X. H.; Yang, F. C.; Qiao, R. Flow of Quasi-Two Dimensional Water in Graphene Channels. *J. Chem. Phys.* **2018**, *148*, 064702.
- 78. Altabet, Y. E.; Haji-Akbari, A.; Debenedetti, P. G. Effect of Material Flexibility on the Thermodynamics and Knetics of Hydrophobically Induced Evaporation of Water. *Proc. Natl. Acad. Sci. U.S.A.* **2017**, *114*, E2548-E2555.
- 79. Cariglia, M.; Giambo, R.; Perali, A. Electronic Properties of Curved Few-Layers Graphene: A Geometrical Approach. *Condensed Matter* **2018**, *3*, 11.
- 80. Tang, Q.; Zhou, Z.; Chen, Z. F. Graphene-Related Nanomaterials: Tuning Properties by Functionalization. *Nanoscale* **2013**, *5*, 4541-4583.
- 81. Mark, P.; Nilsson, L. Structure and Dynamics of the Tip3p, Spc, and Spc/E Water Models at 298 K. J. Phys. Chem. A **2001**, 105, 9954-9960.
- 82. Ojaghlou, N.; Tafreshi, H. V.; Bratko, D.; Luzar, A. Dynamical Insights into the Mechanism of a Droplet Detachment from a Fiber. *Soft Matter* **2018**, *14*, 8924.
- 83. Shafiei, M.; von Domaros, M.; Bratko, D.; Luzar, A. Anisotropic Structure and Dynamics of Water under Static Electric Fields. *J. Chem. Phys.* **2019**, *150*, 074505.
- 84. von Domaros, M.; Bratko, D.; Kirchner, B.; Hummer, G.; Luzar, A. Multifaceted Water Dynamics in Spherical Nanocages. *J. Phys. Chem. C* **2019**, *123*, 5989-5998.
- 85. Daub, C. D.; Cann, N. M.; Bratko, D.; Luzar, A. Electrokinetic Flow of an Aqueous Electrolyte in Amorphous Silica Nanotubes. *Phys. Chem. Chem. Phys.* **2018**, *20*, 27838-27848.

- 86. Choudhuri, J. R.; Vanzo, D.; Madden, P. A.; Salanne, M.; Bratko, D.; Luzar, A. Dynamic Response in Nanoelectrowetting on a Dielectric. *ACS Nano* **2016**, *10*, 8536-8544.
- 87. Shafiei, M.; Ojaghlou, N.; Zamfir, S. G.; Bratko, D.; Luzar, A. Modulation of Structure and Dynamics of Water under Alternating Electric Field and the Role of Hydrogen Bonding. *Mol. Phys.* **2019**, *117*, 3282-3296.
- 88. Malde, A. K.; Zuo, L.; Breeze, M.; Stroet, M.; Poger, D.; Nair, P. C.; Oostenbrink, C.; Mark, A. E. An Automated Force Field Topology Builder (Atb) and Repository: Version 1.0. *J. Chem. Theory Comput.* **2011**, *7*, 4026-4037.
- 89. Stroet, M.; Caron, B.; Visscher, K. M.; Geerke, D. P.; Malde, A. K.; Mark, A. E. Automated Topology Builder Version 3.0: Prediction of Solvation Free Enthalpies in Water and Hexane. *J. Chem. Theory Comput.* **2018**, *14*, 5834-5845.
- 90. Plimpton, S. Fast Parallel Algorithms for Short-Range Molecular-Dynamics. *J. Comput. Phys.* **1995**, *117*, 1-19.
- 91. Evans, D. J.; Holian, B. L. The Nose-Hoover Thermostat. *J. Chem. Phys.* **1985**, *83*, 4069-4074.
- 92. Yeh, I. C.; Berkowitz, M. L. Ewald Summation for Systems with Slab Geometry. *J. Chem. Phys.* **1999**, *111*, 3155-3162.
- 93. Marin-Laflèche, A.; Haefele, M.; Scalfi, L.; Coretti, A.; Dufils, T.; Jeanmairet, G.; Reed, S.; Serva, A.; Berthin, R.; Bacon, C.; Bonella, S.; Rotenberg, B.; Madden, P.A.; Salanne, M. MetalWalls: A Classical Molecular Dynamics Software Dedicated to the Simulation of Electrochemical Systems. ChemRxiv 06/01/2020. https://doi.org/10.26434/chemrxiv.12389777.v1
- 94. Daub, C. D.; Bratko, D.; Luzar, A. Electric Control of Wetting by Salty Nanodrops: Molecular Dynamics Simulations. *J. Phys. Chem. C* **2011**, *115*, 22393-22399.
- 95. de Ruijter, M. J.; Blake, T. D.; De Coninck, J. Dynamic Wetting Studied by Molecular Modeling Simulations of Droplet Spreading. *Langmuir* **1999**, *15*, 7836-7847.
- 96. Taubin, G. Estimation of Planar Curves, Surfaces, and Nonplanar Space-Curves Defined by Implicit Equations with Applications to Edge and Range Image Segmentation. *IEE Trans. Patt. Anal. Machine Intel.* **1991,** *13*, 1115-1138.
- 97. Weijs, J. H.; Marchand, A.; Andreotti, B.; Lohse, D.; Snoeijer, J. H. Origin of Line Tension for a Lennard-Jones Nanodroplet. *Phys. Fluids* **2011**, *23*, 022001.



T.O.C. graphics